Check for updates

Wind-Driven Soft-Contact Rotary Triboelectric Nanogenerator Based on Rabbit Fur with High Performance and Durability for Smart Farming

Jiajia Han, Yawei Feng, Pengfei Chen, Xi Liang, Hao Pang, Tao Jiang,* and Zhong Lin Wang*

Wind energy, as one kind of renewable and sustainable energy sources, is expected to solve the problem of energy consumption and environment deterioration. Here, an improved rotary triboelectric nanogenerator (TENG) using rabbit fur-based soft-contact (SCR-TENG) with segmented structure for harvesting low-speed wind energy is design and fabricated. The adopted soft raw-rabbit fur shows excellent performance in triboelectrification and is beneficial to reducing frictional resistance and prolonging the lifetime of device. After 480 000 cycles, no obvious wear is observed on the dielectric film surface, and the transferred charge is not significantly attenuated. The mechanical-to-electrical energy conversion efficiency of 15.4% can be achieved. Moreover, self-powered applications have been successfully demonstrated in night direction indication, insect trapping, soil moisture detection, ambient temperature and humidity detection, and signal transmission, powered by SCR-TENG, toward smart farming.

1. Introduction

Energy consumption and environment deterioration have aroused widespread concerns of the society.[1–3] Renewable and sustainable energy sources are regarded as a kind of promising solutions to these problems. Wind energy is one of the most pervasive, sustainable, and easily accessible clean renewable energy sources with huge quantity, which is expected to achieve large-scale exploitations and applications. However, current wind energy converters based on the electromagnetic induction are usually bulky, heavy, ineffective at low speeds, and require a dedicated wind farm for installation.[4,5] As reported, the global average wind speed is recorded to be 3.28 m s^{-1} at an observation altitude of 10 m,[6] implying the insufficient collection efficiency of breeze resources in the low-lying terrain by the current power generation technology.[7] Therefore, other energy conversion technologies suitable for the low-frequency breeze wind energy are desirable for overcoming the drawbacks of wind turbine generators.

Based on the coupling effect of triboelectrification and electrostatic induction, triboelectric nanogenerators (TENGs, also called as Wang generators) can effectively convert environmental mechanical energy into electricity, especially for the irregular and distributed vibration energy.[8–11] The TENGs have shown superior output performance over electromagnetic generators in capturing low-frequency discrete energy.[12–14] Due to their merits of high-power density, light weight, low cost, and diversiform materials and structure, they have been applied to effectively harvest the wind energy.[15–18] Sufficient friction between the directly contacted tribo-pair is necessary for generating more tribo-charges and higher output power density for the conventional TENG,[19] but it possibly results in the serious abrasion after long-term operation, lowering the device life cycle.

So far, various efforts have been made to improve the device durability, such as the structural designs of rolling electrification,[20–23] pendulum motion,[10,24,25] dielectric brushes,[12,18,25] and automatic mode switching.[7,26,27] In the previous works, soft-contact operation mode of the TENG has been verified to be an effective strategy for durability improvement.[18,28] Animal furs with softness and elasticity features can maintain tight contact and less resistance when rubbing against another triboelectric layer during cycled operation. By introducing flexible furs into the TENG as triboelectric materials, not only more positive

J. Han, Y. Feng, P. Chen, X. Liang, H. Pang, T. Jiang, Z. L. Wang
CAS Center for Excellence in Nanoscience
Beijing Key Laboratory of Micro-Nano Energy and Sensor
Beijing Institute of Nanoenergy and Nanosystems
Chinese Academy of Sciences
Beijing 101400, P. R. China
E-mail: jiangtao@binn.cas.cn
J. Han, Y. Feng, P. Chen, X. Liang, T. Jiang, Z. L. Wang
School of Nanoscience and Technology
University of Chinese Academy of Sciences
Beijing 100049, P. R. China
H. Pang, T. Jiang
School of Chemistry and Chemical Engineering
Guangxi University
Nanning, Guangxi 530004, P. R. China
T. Jiang, Z. L. Wang
CUSTech Institute of Technology
Wenzhou, Zhejiang 325024, P. R. China
Z. L. Wang
School of Materials Science and Engineering
Georgia Institute of Technology
Atlanta, GA 30332-0245, USA
E-mail: zlwang@gatech.edu

tribo-charges are injected onto the dielectric surface, but also the material wear is greatly reduced. The external driving force can be greatly lowered, along with the enhanced output density and increased device durability.

In this paper, an improved soft-contact rotary TENG (SCR-TENG) with segmented structure for harvesting low-speed wind energy was design and fabricated. Elastic and soft rabbit fur was adopted as the typical triboelectric material, and a shaft-bearing structure transmitted the wind energy collected by the wind cups to the TENG, converting the captured mechanical energy into electricity. The contact state of fur brushes and fluorinated ethylene propylene (FEP) films was controlled by adjusting the gap distance between the brushes and the electrodes. Compared with various hard-contact competitors, the SCR-TENG exhibits more transferred charges, higher output performance and more excellent durability at the same torque and rotation speed, which means that weak discrete kinetic energy in the environment can be used to its greatest extent by the designed device. At the gap of 7 mm, the segmented SCR-TENG generates the optimal electrical outputs, and the starting wind speed for a 36-grid TENG gets close to 1 m s^{-1}, indicating a wide range of wind speeds that can be collected. Successful demonstrations on night direction indication, insect trapping, soil moisture detection, ambient temperature, and humidity detection and signal transmission by converting wind energy showed the potential applications of the SCR-TENG in smart farming.

2. Results and Discussion

2.1. Principle of the Designed SCR-TENG

The tribo-pair of a common TENG (such as polymer against metal) is mostly manipulated by the sufficient contact to improve the surface charge density for better output performance. In this case, due to the great frictional resistance between the tribo-pair, severe material wear will be caused during the relative motion. The TENGs operating in a soft-contact mode can solve the above problem. A flexible charge injection mechanism is introduced to separate the stator and rotor, which not only greatly reduces the frictional resistance of TENG during operation, protects the surface of the charged dielectric layer, prolongs the device life, but also greatly improves the output power density of the TENG. The structural comparison of soft-contact and direct-contact TENGs is schematically shown in **Figure 1**a. The direct-contact TENG uses the copper electrode to directly rub with the polymer for electrification, as an example, while the SCR-TENG is composed of rabbit fur and polymer, based on the freestanding mode.

The power generation of the SCR-TENG is based on the triboelectrification between different materials and electrostatic induction. During the operation process under external mechanical triggering, the FEP films and the fan-shaped fur brushes are in good contact for electron transfer, generating opposite net electrostatic charges on their surfaces until the saturated state (Figure 1b). The saturated tribo-charge amounts on the rotor (positive charges on the fur sectors) and stator (negative charges on the FEP films) are equivalent, but the

charge density on the FEP is half of that on the fur brushes for the doubled area. Figure S1, Supporting Information, presents the charge accumulation process of the SCR-TENG at the short-circuit state (Q_{SC}). The surface charge of the FEP films gets saturated after 120 s of continuous external mechanical stimulation.

The power generation mechanism of the SCR-TENG is schematically illustrated in Figure 1c. The state (i), where the fur brush is placed exactly above the right electrode, is taken as the initial condition. Appropriate negative free charges are induced on the right electrode to shield the excessive positive-polarization above it. As the fur sector revolves clockwise relative to the fixed electrodes (states i–v), the intensity of the positive-polarization above the right electrode decreases, but the positive-polarization above the left electrode increases. As a result, free charges on both electrodes will be redistributed by this driving force via the electron transfer from the right electrode to left one, generating a current from the left electrode to the right one across the external circuit. After the fur sector passes a whole electrode (states v–viii), the electrons flow backward to the right electrode, generating a reversed current pulse through the external resistance. The constant rotation produces continuous AC output of the SCR-TENG.

2.2. Optimization of the SCR-TENG

The output performance of the SCR-TENG was optimized starting from the fur brush fixing method on a standardized dynamic torque measurement system (**Figure 2**a). The rotation speed of the rotor was controlled to be 60 rpm. The length of brush hair is ≈20 mm, and they can be spread out along the growth direction without any intervention. Two different fixing methods, that is, directly pasting on an acrylic disk and framed by an acrylic mold (Figure 2b), were adopted. Figure 2c,d presents the comparison of transferred charge (Q_{SC}) and short-circuit current (I_{SC}) of the SCR-TENG using different rotors under various torques. As the torque increases from 20 to 90 mN m, the contact between rabbit fur and FEP becomes closer, and the short-circuit charge and current gradually increase. The column graph of Figure 2c indicates the amount of transferred charges for the rotor disk without a framework is more than that with a framework. The used rotors with two different fixing methods are presented in Figure S2a,b, Supporting Information. Compared to the rabbit furs without the fixed frame, where the furs are scattered and have larger contact area with FEP, the framed furs remain upright after testing, and the boundaries between different grids are clear and not overlapped (Figure S2c,d, Supporting Information). Moreover, the short-circuit current of the TENG with a fixed frame is always higher than that without a frame.

Enlarged views of a pulse peak of the short-circuit charge and current for the rotor disks with or without the frame are shown in Figure S2e,f, Supporting Information, indicating that the waveforms of the transferred charges are basically the same, but those of the current are quite different. The output current peak by the rotor disk with a fixed frame is a sharp peak, while the current peak without a frame is a flat peak.
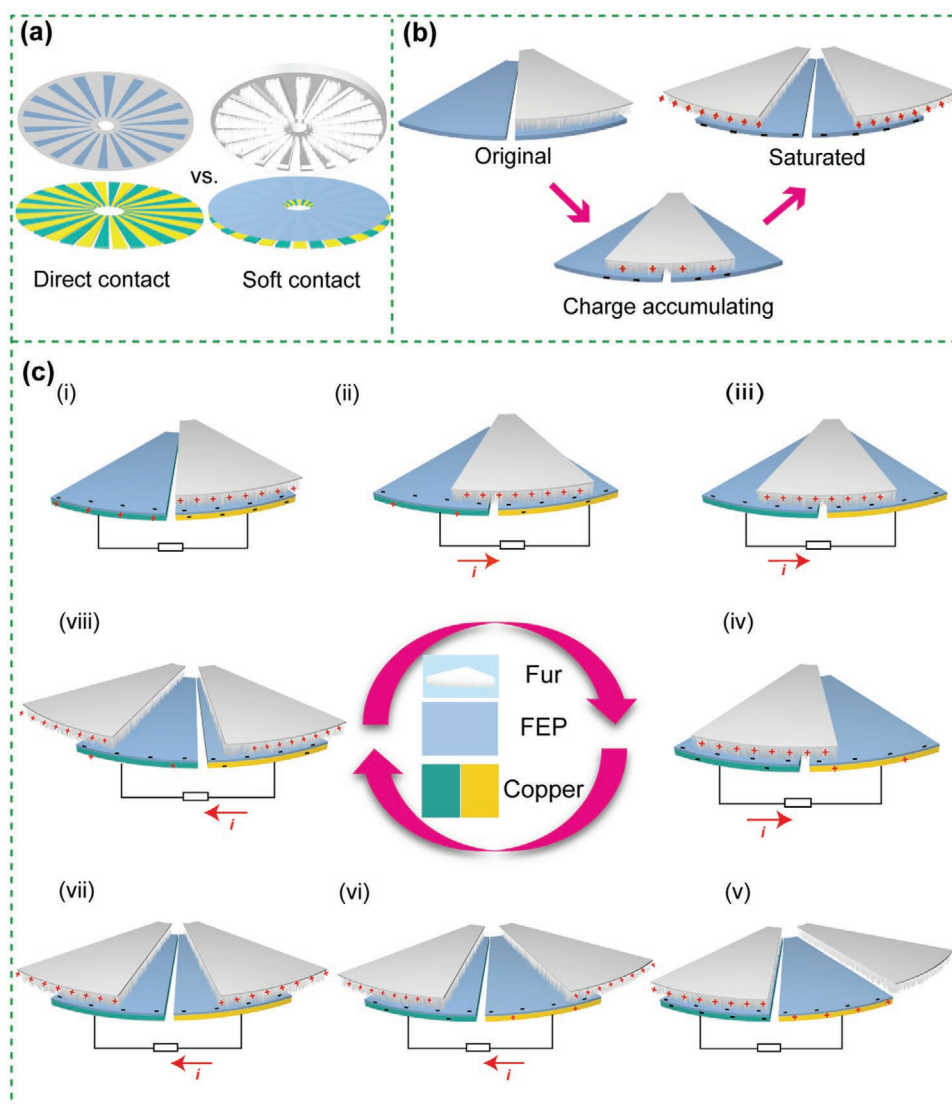
Figure 1. Schematic diagram showing the working principle of the SCR-TENG. a) The comparison of the direct-contact and soft-contact rotational TENGs. Schematic operation principle of the SCR-TENG for b) triboelectrification in charge accumulation process and c) electrostatic induction in charge-saturated stage.

The time integral value of the current for a rotor disk without a frame is larger than that with a frame (Figure 2e,f), that is, the transferred charge is larger. In addition, the trimmed rabbit furs were also used for comparison. The short-circuit transferred charge and current for the raw and mowed rabbit furs are presented in Figure 2g,h. The mowed rabbit furs have a length of ≈5 mm, and the softness is reduced compared with untreated rabbit furs, which may be the main cause of the decrease in charge and current. According to the enlarged view of a pulse peak of short-circuit current (Figure S3a–d, Supporting Information), the current waveform for the mowed rabbit fur exhibits a flat peak, resulting in smaller current relative to the case of raw rabbit fur, but basically equivalent transferred charge amount.

In order to select a suitable tribo-pair with the best performance, we have chosen several common material combinations, including FEP versus copper, polytetrafluoroethylene

(PTFE) versus rabbit fur, and FEP versus rabbit fur (**Figure 3**a,b). According to the results of transferred charge and short-circuit current, the combination of FEP and rabbit fur presents excellent electrification performance. The combination of FEP and copper also produces more charges at low torque, but at the end of the test, the FEP surface is visibly damaged (Figure S4, Supporting Information). The deep scratches on the FEP surface can be observed by an optical microscope. The FEP film and Cu are in direct contact with large frictional force, resulting in serious material wear. However, for the FEP-rabbit fur combination, there is almost no remarkable decrease in the output performance after 480 000 cycles (Figure 3c,d).

The optical microscope images in Figure 3e,f show that there is little difference between the surfaces of unused FEP film and used FEP film, and only a few streaks appear on the FEP surface after use. Additionally, the surfaces of the FEP
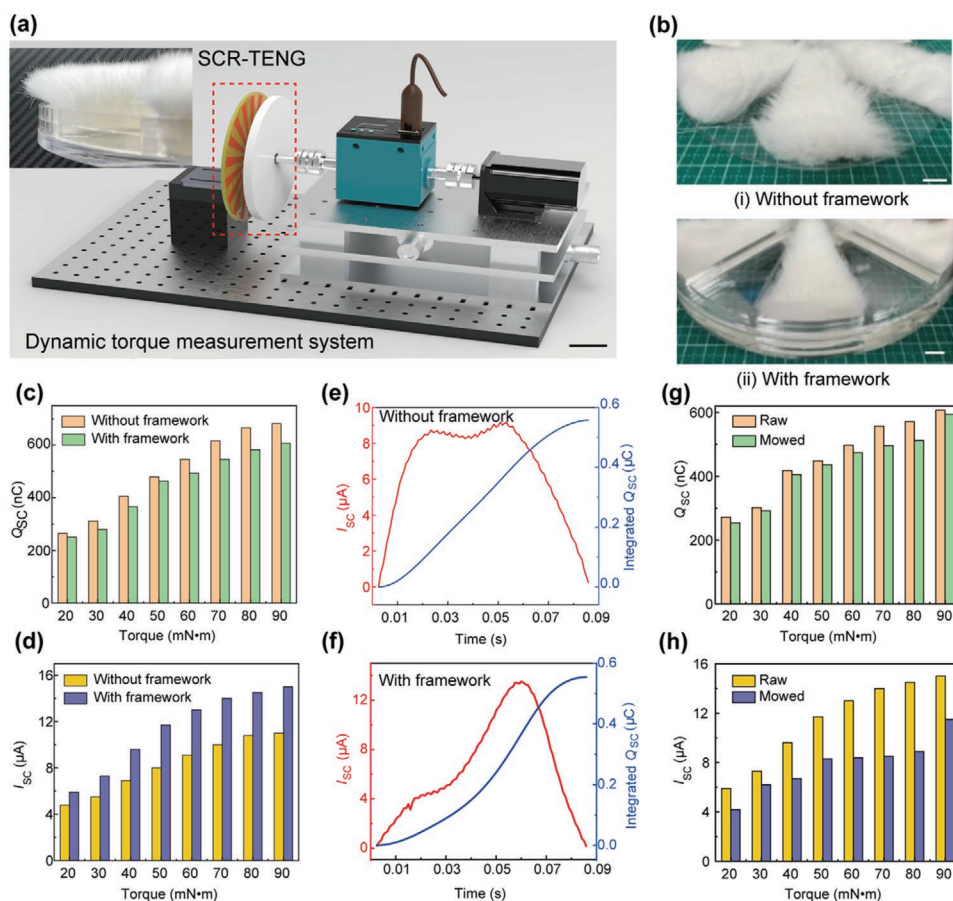
Figure 2. Performance optimization of the SCR-TENG. a) Schematic diagram showing the dynamic torque measurement system for the SCR-TENG performance optimization. The inset is the partial amplified image of rabbit fur. The scale bar is 5 cm. b) Photographs showing the rotors with fur brushes without and with framework. The scale bar is 1 cm. c) Q_{SC} and d) I_{SC} from different SCR-TENGs under various torques. Half-periodic pulse wave of the SCR-TENG using the rotors e) without and f) with brush framework. The comparison of g) Q_{SC} and h) I_{SC} from the framed SCR-TENG with raw and mowed fur brushes under various torques.

films before and after use were also characterized by the atomic force microscope (AFM), as illustrated in Figure 3g,h. A slight change in the height of the FEP film after use may be due to the pulling of the FEP film during the sampling process. Furthermore, the effects of rotating speed and grating number were also investigated, as shown in Figure S5, Supporting Information. It is apparent that the transferred charges are almost unchanged, as the rotating speed increases from 30 to 120 rpm. But the short-circuit current is increased to 15 µA. Similarly, with increasing the grating number, the output current is also raised (Figure S5c,d, Supporting Information). After considering these factors, we selected the configuration of raw rabbit furs without any treatment and fixed with a framework in the following experiments.

2.3. Performance of the Wind-Driven SCR-TENG

Subsequently, a shaft nesting bearing was used to transmit the wind energy collected by the wind cups to the TENG, which converts the captured mechanical energy into electrical energy. **Figure 4**a presents the photograph of fully assembled

TENG device powered by the wind blowing. There are six evenly distributed air cups above the SCR-TENG part. They are threaded and fixed with stainless steel shafts and bearings. The moment arms of the cups approximately have a length of 225 mm to allow a lower starting wind speed. The structural details of the SCR-TENG are visualized in Figure 4b, in which the sector furs are attached to the acrylic substrate forming a circle, and the copper electrodes fabricated by the printed circuit board (PCB) technology are covered with a layer of FEP film.

The influences of the performed wind speed and the gap distance between the rotor disk and the FEP on the output performance of the SCR-TENG were investigated (Figure 4c–f and Figure S6, Supporting Information). The results show that the TENG with 36-grid electrodes and a gap of 7 mm can generate the optimal output performance at the wind speed of 6 m s^{-1}. As the rotational speed of SCR-TENG increases with the increase of wind speed, the output current and transferred charge will also increase. Under this experimental condition, the wind speed of 6 m s^{-1} is the maximum wind speed we adopted, and the outputs get the optimal values at this speed. In addition, the increase in the number of grids also increases
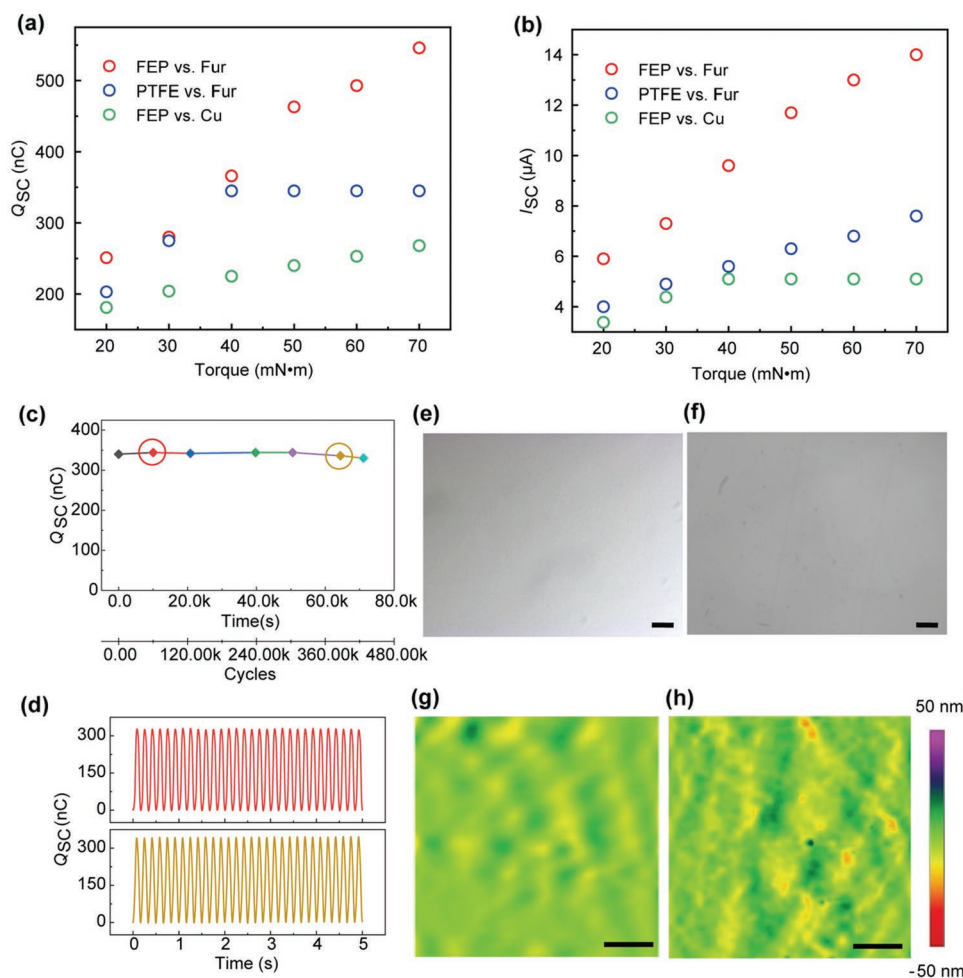
**ADVANCED
SCIENCE NEWS**

www.advancedsciencenews.com

**ADVANCED
FUNCTIONAL
MATERIALS**

www.afm-journal.de

Figure 3. Material selection and durability of the SCR-TENG. a) Q_{SC} and b) I_{SC} comparison of the SCR-TENGs with various tribo-pairs. c) Durability test of the SCR-TENG with the tribo-pair of FEP films and fur brushes for 480 000 cycles of operation. d) Enlarged view of the Q_{SC} variation. The upper waveform indicates the red-point-marked result, while the bottom waveform indicates the yellow-color-marked point in (c). e,f) Optical microscope and g,h) AFM morphology changes of the FEP films e,g) before and f,h) after long-term usage. The scale bars in (e) and (f) represent 10 µm, while the scale bars in (g) and (h) represent 1 µm.

the output current of TENG.[29] In this experiment, for the maximum grid number of 36, the TENG generates the best outputs. So it is reasonable to speculate that better outputs can be achieved for higher wind speed and more grids under the performed conditions. The gap of 7 mm is the optimal gap for the TENG to reach the maximum outputs, through investigating the gap dependence of the starting wind speed and output performance. When the gap distance is less than 7 mm, the frictional resistance between rabbit fur and FEP increases, and the starting wind speed of the TENG also increases. By contrast, when the gap distance is more than 7 mm, the contact between rabbit fur and FEP is not sufficient, and the corresponding output will decrease.

The electrical outputs when loading a resistor were also characterized, and the peak current–resistance and peak power–resistance relationships are depicted in Figure 4g and Figure S7, Supporting Information. The instantaneous output power is calculated by:

$$P = I_t^2 R \tag{1}$$

where R is the loaded resistance and I_t is the instantaneous current across the resistance. As can be seen in Figure 4g, the instantaneous peak power reaches its maximum value of 11.9 mW at the matched resistance of 300 MΩ. The converted electric energy at this resistance for one excitation is obtained by:

$$W = \int_0^T I_t^2 R \, dt \tag{2}$$

where T is the operation duration of the cylindrical TENG. A total electric energy of 3.6 mJ was ultimately converted at the efficiency of 15.4% (Note S1, Supporting Information). Figure 4h,i shows the charging capability of the SCR-TENG device to a capacitor. For a capacitor of 1000 µF, the charging voltage curves at different wind speeds are plotted in Figure 4h. At the wind speed of 6 m s⁻¹, the capacitor can be charged to ≈1.3 V in 120 s. For different capacitors of 100, 330, 550, and 1000 µF, the voltage can arrive at 5.2, 1.6, 1.0, and 0.5 V within 60 s, respectively (Figure 4i).
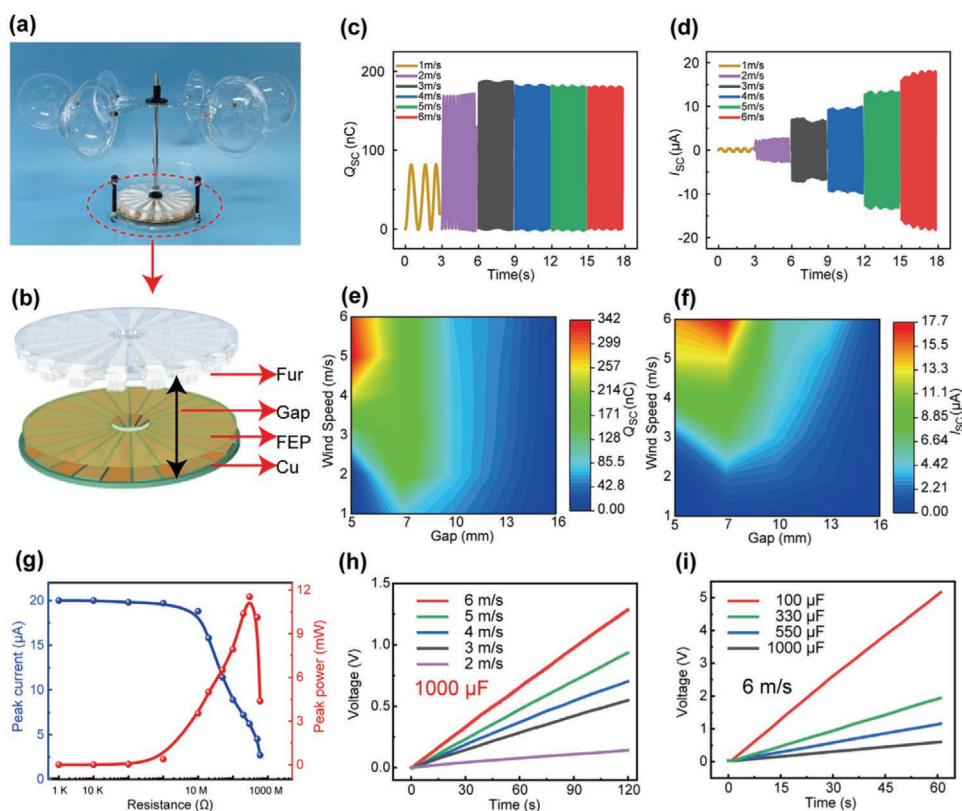
**ADVANCED
SCIENCE NEWS**

www.advancedsciencenews.com

**ADVANCED
FUNCTIONAL
MATERIALS**

www.afm-journal.de

Figure 4. Performance of the wind-driven SCR-TENG. a) A photograph showing the assembled wind-driven SCR-TENG and b) the details of the TENG component. c) Q_{SC} and d) I_{SC} waveforms of the wind-driven SCR-TENG with the internal gap of 7 mm in wind. Hot-zone maps showing e) Q_{SC} and f) I_{SC} of the SCR-TENG with different internal gaps at different wind speeds. g) Instantaneous peak current and power-resistance relationship profiles for the SCR-TENG at the wind speed of 6 m s^{-1}. Charging performance h) to 1000 µF at different wind speeds and i) to various capacitors at the fixed speed of 6 m s^{-1}.

2.4. Application of the Wind-Driven SCR-TENG in Smart Farming

The applications of the SCR-TENG in the smart farming were demonstrated (**Figure 5**a). The construction and development of modern farms requires the integration of information technology, internet of things, and other means to achieve more convenient, accurate, and comprehensive control. According to the geographical location and conditions of farm distribution, the wind-driven TENG can be widely distributed and used in smart farms. For example, large-scale SCR-TENG arrays can be placed in open areas with good air flow, such as roofs, hillsides, etc.

The first application demonstration is a night direction indication in the farm through lighting multiple lights emitting diodes (LEDs) with different patterns by the SCR-TENG. As presented in Figure 5b, 27 LEDs with a diameter of 5 mm were assembled to form an arrow indicating the right direction at different wind speeds (Video S1, Supporting Information). Then, inspired by commercial mosquito traps, we tried to light UV lamps by using the TENG to trap mosquitoes or other moths (Figure 5c). Because the insects are phototropic, we can use their preference for certain wavelengths of ultraviolet to lure them into an insect chamber, where they will die of dehydration.

Crops are important parts on a farm, and water is indispensable in the growing process of crops. Another application demonstration is a self-powered soil moisture sensing powered by the SCR-TENG, as schematically illustrated in Figure S8, Supporting Information. The soil moisture sensor is powered by the TENG. In dry soil, the sensor starts to work and sends a signal to the controller, which controls the pump to work, thus realizing automatic irrigation. When the sensor comes into contact with the water, it transmits the signal to the pump again to stop working. The working process of the sensor and the pump is shown in Video S2, Supporting Information. A 100 µF capacitor was used for electrical energy storage. When it was charged to 5 V, the switch was turned on to make the sensor connected and work normally. The typical voltage curve on the capacitor for the charging and discharging process is shown in Figure 5d.

Finally, the application of temperature and humidity monitoring on the farms was demonstrated. The SCR-TENG was applied to successfully power a commercial thermohygrometer with Bluetooth transmission function, which can send the signals to a mobile phone (Figure 5e). A 1.8 mF capacitor was used as a temporary energy storage unit to supply power to the thermohygrometer. The temperature and humidity data can be received and recorded in the mobile phone APP, matched with the commercial thermohygrometer.
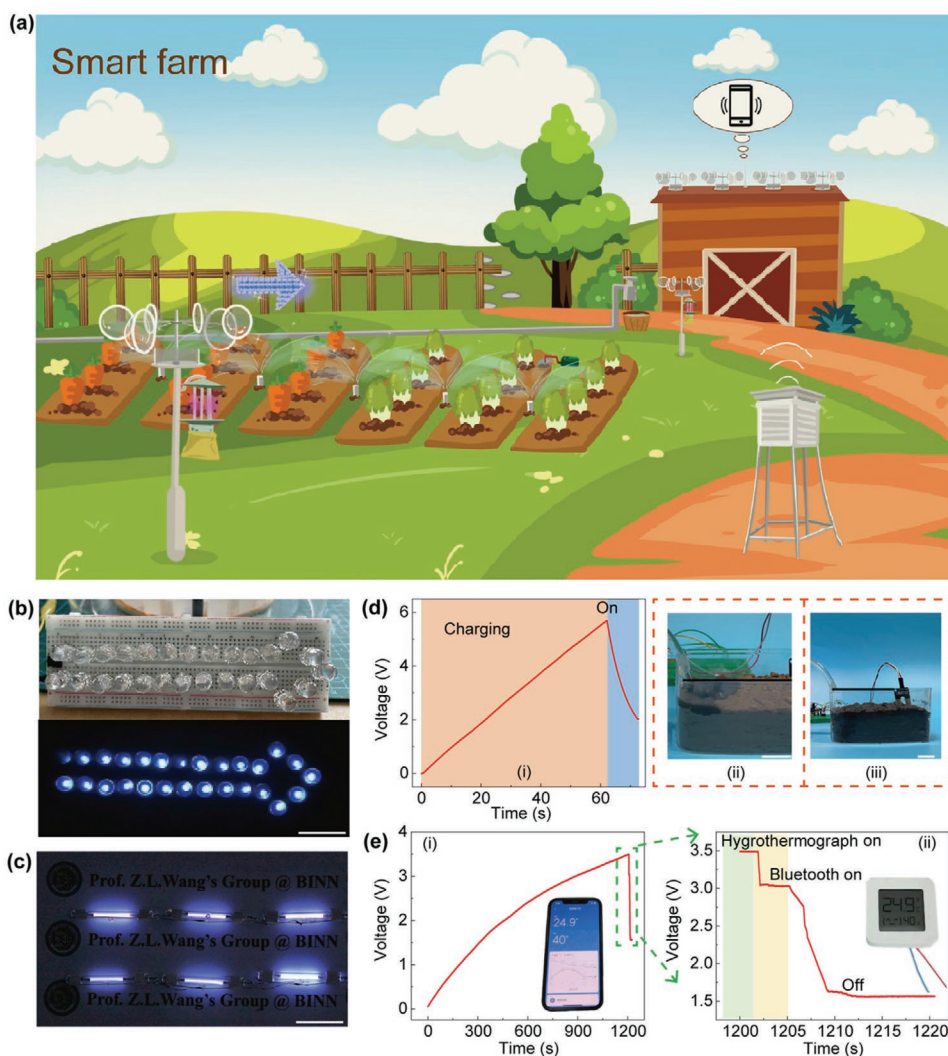
Figure 5. The application of the wind-driven SCR-TENG on smart farming. a) A schematic illustration showing the proposed SCR-TENG in the smart farm. Directly powering b) LED bulbs for direction indication in night and c) glowing UV lamps for mosquito killing by the wind-driven SCR-TENG. d) Application of an automatic irrigation system by charging a 100 µF capacitor. The curve in the left part of (d) showing the voltage change on the capacitor when the system starts working, while the right photograph showing the working system during the marked period in the left graph. e) A wireless environmental data transceiving system achieved by the wind-driven SCR-TENG via charging a 100 µF capacitor. The dramatic voltage drops indicate the normal working of thermal sensor and LED screen, bluetooth. The scale bars in (b) and (c) represent 3 cm, while the scale bars in d(ii) and d(iii) represent 2 cm.

3. Conclusion

In summary, a rabbit fur-based SCR-TENG was fabricated for harvesting wind energy in smart farming application. The framed raw-rabbit furs not only generate high density charges onto the FEP film surface, but also reduce the friction resistance and improve the device durability. After 480 000 operation cycles, there is no obvious wear on the FEP surface and no obvious attenuation for the transferred charges, and the conversion efficiency of 15.4% from the mechanical energy to electrical energy can be achieved. Furthermore, based on the optimized SCR-TENG, a smart farm was built in night indication, mosquito trapping, self-powered sensing of soil moisture, and temperature/humidity monitoring. This work can provide a promising strategy for improving the durability at low wind speed and developing smart farm conveniently.

4. Experimental Section

Fabrication of the SCR-TENG: For the rotating part of the SCR-TENG, the whole pieces of rabbit fur with uniform hair length and density purchased from the retailer were cut into sectors of 28, 13, or 9 degrees with the length of 20 mm by a laser cutting machine. Then double-sided tape (3M LSE) was used to attach it on an acrylic or 3D printed polylactic acid substrate disk with grooves. For the stator part, copper electrodes were deposited on a disk-shaped RF4 glass fiber board with a diameter of 177 mm. Several types of complementary electrodes with different grid numbers were designed, and gaps of ≈1 mm were reserved between the adjacent electrodes. Two groups of copper sectors were respectively connected and two wires were drawn on the back of the PCB as output terminals. The surfaces of the Cu electrodes were covered by a polymer layer (FEP, PTFE, or Kapton) for electrostatic induction.

Electric Measurements of the TENG Device: A Keithley 6514 system electrometer was used to test the transferred charge (Q_{SC}) and current (I_{SC}) of the device under the short circuit state. The torque was measured

by a commercial torque sensor (DYN-200). For the performance under the driven of wind, a wind turbine system (SHF-2.5A) was applied to precisely control the generated wind, and an anemometer (THINRAD TA-1) was used to record the wind speed.

Supporting Information

Supporting Information is available from the Wiley Online Library or from the author.

Acknowledgements

Conflict of Interest

The authors declare no conflict of interest.

Data Availability Statement

Research data are not shared.

Keywords

[1] W. Zhong, L. Xu, X. Yang, W. Tang, J. Shao, B. Chen, Z. L. Wang, *Nanoscale* **2019**, *11*, 7199.

[2] X. Liang, Y. Feng, P. Lu, J. An, T. Jiang, Z. L. Wang, *Adv. Energy Mater.* **2020**, *10*, 2002123.

[3] A. Ahmed, I. Hassan, M. F. El-Kady, A. Radhi, C. K. Jeong, P. R. Selvaganapathy, J. Zu, S. Ren, Q. Wang, R. B. Kaner, *Adv. Sci.* **2019**, *6*, 1802230.

[4] G. Lalor, A. Mullane, M. O'Malley, *IEEE Trans. Power Syst.* **2005**, *20*, 1905.

[5] M.-S. Kang, *IEEE Trans. Energy Convers.* **2007**, *22*, 397.

[6] C. Jung, D. Schindler, *Sustainable Energy Technol. Assess.* **2020**, *42*, 100852.

[7] S. Yong, J. Wang, L. Yang, H. Wang, H. Luo, R. Liao, Z. L. Wang, *Adv. Energy Mater.* **2021**, *11*, 2101194.

[8] X. Liang, T. Jiang, G. Liu, Y. Feng, C. Zhang, Z. L. Wang, *Energy Environ. Sci.* **2020**, *13*, 277.

[9] Y. Feng, T. Jiang, X. Liang, J. An, Z. L. Wang, *Appl. Phys. Rev.* **2020**, *7*, 021401.

[10] T. Jiang, H. Pang, J. An, P. Lu, Y. Feng, X. Liang, W. Zhong, Z. L. Wang, *Adv. Energy Mater.* **2020**, *10*, 2000064.

[11] J. Cheng, W. Ding, Y. Zi, Y. Lu, L. Ji, F. Liu, C. Wu, Z. L. Wang, *Nat. Commun.* **2018**, *9*, 3733.

[12] Y. Feng, X. Liang, J. An, T. Jiang, Z. L. Wang, *Nano Energy* **2021**, *81*, 105625.

[13] P. Lu, H. Pang, J. Ren, Y. Feng, J. An, X. Liang, T. Jiang, Z. L. Wang, *Adv. Mater. Technol.* **2021**, 2100496.

[14] Y. Zhong, H. Zhao, Y. Guo, P. Rui, S. Shi, W. Zhang, Y. Liao, P. Wang, Z. L. Wang, *Adv. Mater. Technol.* **2019**, *4*, 1900741.

[15] C. Ye, K. Dong, J. An, J. Yi, X. Peng, C. Ning, Z. L. Wang, *ACS Energy Lett.* **2021**, *6*, 1443.

[16] H. Lin, M. He, Q. Jing, W. Yang, S. Wang, Y. Liu, Y. Zhang, J. Li, N. Li, Y. Ma, L. Wang, Y. Xie, *Nano Energy* **2019**, *56*, 269.

[17] Y. Xie, S. Wang, L. Lin, Q. Jing, Z. Lin, S. Niu, Z. Wu, Z. L. Wang, *ACS Nano* **2013**, *7*, 7119.

[18] P. Chen, J. An, S. Shu, R. Cheng, J. Nie, T. Jiang, Z. L. Wang, *Adv. Energy Mater.* **2021**, *11*, 2003066.

[19] W. He, W. Liu, J. Chen, Z. Wang, Y. Liu, X. Pu, H. Yang, Q. Tang, H. Yang, H. Guo, C. Hu, *Nat. Commun.* **2020**, *11*, 4277.

[20] L. Liu, X. Yang, L. Zhao, H. Hong, H. Cui, J. Duan, Q. Yang, Q. Tang, *ACS Nano* **2021**, *15*, 9412.

[21] L. Liu, Q. Shi, C. Lee, *Nano Energy* **2020**, *76*, 105052.

[22] A. Ahmed, Z. Saadatnia, I. Hassan, Y. Zi, Y. Xi, X. He, J. Zu, Z. L. Wang, *Adv. Energy Mater.* **2016**, *6*, 1601705.

[23] Y. Pang, S. Chen, Y. Chu, Z. L. Wang, C. Cao, *Nano Energy* **2019**, *66*, 104131.

[24] Z. Lin, B. Zhang, H. Guo, Z. Wu, H. Zou, J. Yang, Z. L. Wang, *Nano Energy* **2019**, *64*, 103908.

[25] Z. Lin, B. Zhang, Y. Xie, Z. Wu, J. Yang, Z. L. Wang, *Adv. Funct. Mater.* **2021**, *31*, 2105237.

[26] H. Yang, M. Deng, Q. Zeng, X. Zhang, J. Hu, Q. Tang, H. Yang, C. Hu, Y. Xi, Z. L. Wang, *ACS Nano* **2020**, *14*, 3328.

[27] J. Chen, H. Guo, C. Hu, Z. L. Wang, *Adv. Energy Mater.* **2020**, *10*, 2000886.

[28] P. Chen, J. An, R. Cheng, S. Shu, A. Berbille, T. Jiang, Z. L. Wang, *Energy Environ. Sci.* **2021**, *14*, 4523.

[29] L. Long, W. Liu, Z. Wang, W. He, G. Li, Q. Tang, H. Guo, X. Pu, Y. Liu, C. Hu, *Nat. Commun.* **2021**, *12*, 4689.